Journal of Solid State Chemistry 182 (2009) 1798–1805

Contents lists available at ScienceDirect

Journal of Solid State Chemistry

journal homepage: www.elsevier.com/locate/jssc

Hydrothermal syntheses, crystal structures and properties of 0-D, 1-D and 2-D organic–inorganic hybrid borotungstates constructed from Keggin-type heteropolyanion $[\alpha\text{-}BW_{12}O_{40}]^{5-}$ and transition-metal complexes

Junwei Zhao, Yiping Song, Pengtao Ma, Jingping Wang *, Jingyang Niu *

Institute of Molecular and Crystal Engineering, College of Chemistry and Chemical Engineering, Henan University, Kaifeng 475004, China

ARTICLE INFO

Article history:
Received 25 December 2008
Received in revised form
18 April 2009
Accepted 22 April 2009
Available online 3 May 2009

Keywords:
Polyoxometalates
Hydrothermal synthesis
Keggin structure
Transition metal complex

ABSTRACT

Three novel organic–inorganic hybrid borotungstates $\{[Ni(phen)_2(H_2O)]_2H(\alpha\text{-}BW_{12}O_{40})\}\cdot 4H_2O$ (**1**), $[Cu^I(2,2'\text{-bipy})(4,4'\text{-bipy})_{0.5}]_2\{[Cu^I(2,2'\text{-bipy})]_2Cu^I(4,4'\text{-bipy})_2(\alpha\text{-}BW_{12}O_{40})\}$ (**2**) and $\{[Cu^I(4,4'\text{-bipy})]_3H_2(\alpha\text{-}BW_{12}O_{40})\}\cdot 3.5H_2O$ (**3**) (phen = 1,10-phenanthroline, 2,2′-bipy = 2,2′-bipyridine, 4,4′-bipy = 4,4′-bipyridine) have been hydrothermally synthesized and structurally characterized by elemental analyses, IR, UV spectra, powder X-ray diffraction (PXRD), thermogravimetric analysis (TGA), single-crystal X-ray diffraction, X-ray photoelectron spectroscopy (XPS) and photoluminescence. The structural analysis reveals that **1** consists of a 0-D bisupporting polyoxometalate cluster where two $[Ni(phen)_2(H_2O)]^{2+}$ cations are grafted on the polyoxoanion $[\alpha\text{-}BW_{12}O_{40}]^{5-}$ through two terminal oxygen atoms, **2** shows a 1-D infinite chain constructed from $[\alpha\text{-}BW_{12}O_{40}]^{5-}$ polyoxoanions and $\{[Cu^I(2,2'\text{-bipy})]_2Cu^I(4,4'\text{-bipy})_2\}^{3+}$ cations by means of alternating fashion, and **3** displays an unprecedented 2D extended structure built by $[\alpha\text{-}BW_{12}O_{40}]^{5-}$ polyoxoanions and $-Cu^I\text{–}4,4'\text{-bipy}-$ linear chains, in which each $[\alpha\text{-}BW_{12}O_{40}]^{5-}$ polyoxoanion acts as a tetradentate inorganic ligand and provides three terminal oxygen atom and one two-bridging oxygen atom. The presence of Ni^{II} and W^{VI} in **1**, Cu^I ions and W^{VI} in **2** and **3** are identified by XPS spectra. The photoluminescence of **2** and **3** are also investigated.

1. Introduction

Polyoxometalates (POMs) bear many intriguing properties which make them attractive for applications in catalysis, biology, magnetism, optics and medicine [1–5]. In this context, there has been an increasing interest in constructing functionalized POM-based organic–inorganic hybrid materials through grafting of organic or metal-organic moieties on the surface oxygen atoms from POM moieties [6–9]. One very effective designed route to gain such functionalized POM materials is that use interesting POMs as building blocks, and then link them up using organic molecules or secondary metal-organic complexes as bridging groups [10–33]. Among the different types of POM polyoxoanions, the most useful polyoxoanions are the classical Keggin-type polyoxoanions [34–35]. Up to now, a series of POM-based organic–inorganic hybrids consisting of Keggin polyoxoanions and various metal-organic complexes or organic substrates have been reported [25–38]. However, it is noticeable that the organic–inorganic hybrid POM-based materials containing Keggin-type borotungstate polyoxoanions as building blocks are still very limited. Therefore, the continuous exploration and investigations on borotungstate-based hybrid materials in which boron-centered tungsten–oxygen heteropolyanions as building blocks are very necessary and interesting for their potential values [39–41]. In 2004, we firstly reported a novel 2-D network organic–inorganic hybrid compound $(dmaH)_2[Nd(dmf)_4(H_2O)][\alpha\text{-}BW_{12}O_{40}]\cdot H_2O$ (dma = dimethylamine, dmf = N,N-dimethylformamide) constituted by $[Nd(dmf)_4(H_2O)]^{3+}$ cations and Keggin-type $[\alpha\text{-}BW_{12}O_{40}]^{5-}$ polyoxoanions [42]. Two years later, we also addressed an isostructural cerium species $(dmaH)_2[Ce(dmf)_4(H_2O)][\alpha\text{-}BW_{12}O_{40}]\cdot H_2O$ [43]. In 2006, Wang et al. communicated a couple of enantiomerically pure 3-D architectures $KH_2[(D\text{-}C_5H_8NO_2)_4(H_2O)Cu_3]$ $[\alpha\text{-}BW_{12}O_{40}]\cdot 5H_2O$ and $KH_2[(L\text{-}C_5H_8NO_2)_4(H_2O)Cu_3][\alpha\text{-}BW_{12}O_{40}]\cdot 5H_2O$ with helical channels constructed from $[\alpha\text{-}BW_{12}O_{40}]^{5-}$ clusters and copper-amino acid complexes, which show significant induced optical activity in the POM moieties as a result of chirality transfer from the chiral proline molecules to the whole framework [44]. In 2007, Wang et al. again synthesized a functionalized borotungstate by hexanuclear copper-amino acid coordination complexes $H_4[Na(H_2O)_2][Cu_6Na(gly)_8(H_2O)_2][\alpha\text{-}BW_{12}O_{40}]_2\cdot 13H_2O$ [45]. Recently, we addressed three inorganic–organic borontungstates supported by transition-metal–organic complexes $[Mn(2,2'\text{-bipy})_3]_{1.5}[BW_{12}O_{40}Mn(2,2'\text{-bipy})_2(H_2O)]\cdot 0.25H_2O$, $[Fe(2,2'\text{-bipy})_3]_{1.5}[BW_{12}O_{40}Fe(2,2'\text{-bipy})_2(H_2O)]\cdot 0.5H_2O$ and $[Cu_2(phen)_2(OH)_2]_2H[Cu(H_2O)_2\{BW_{12}O_{40}Cu_{0.75}(phen)(H_2O)\}_2]\cdot 1.5H_2O$ [46]. As a

* Corresponding authors. Fax: +86 378 3886876.
E-mail addresses: jpwang@henu.edu.cn (J. Wang), jyniu@henu.edu.cn (J. Niu).

0022-4596/$ - see front matter © 2009 Elsevier Inc. All rights reserved.
doi:10.1016/j.jssc.2009.04.028

Table 1
Crystallographic data and structure refinements for **1**–**3**.

	1	**2**	**3**
Empirical	$C_{48}H_{45}N_8Ni_2BW_{12}O_{46}$	$C_{70}H_{56}N_{14}Cu_5BW_{12}O_{40}$	$C_{30}H_{33}N_6Cu_3BW_{12}O_{43.5}$
Formula weight	3804.175	4268.00	3581.18
T (K)	296(2)	296(2)	296(2)
Crystal system	Triclinic	Triclinic	Triclinic
Space group	P-1	P-1	P-1
a (Å)	11.2965(6)	13.779(3)	12.7043(7)
b (Å)	13.5334(7)	14.154(3)	13.6868(7)
c (Å)	13.5538(7)	14.472(3)	18.4722(10)
α (°)	67.9540(10)	63.838(3)	89.7990(10)
β (°)	74.7330(10)	86.871(3)	86.3030(10)
γ (°)	69.0290(10)	65.200(3)	74.7280(10)
V (Å^3)	1773.36(16)	2270.1(7)	3091.8(3)
Z	1	1	2
D_c (g cm^{-3})	3.550	3.122	3.837
μ (mm^{-1})	19.994	16.366	23.329
Crystal size (mm^3)	0.19 × 0.15 × 0.13	0.18 × 0.15 × 0.12	0.17 × 0.12 × 0.09
θ Range for data collections	1.64–25.00°	1.59–25.00	1.67–25.00
Limiting indices	$-13 \le h \le 11$	$-13 \le h \le 16$	$-15 \le h \le 15$
	$-16 \le k \le 13$	$-6 \le k \le 16$	$-16 \le k \le 16$
	$-16 \le l \le 14$	$-12 \le l \le 17$	$-21 \le l \le 21$
Reflections collected	9141	10 507	30 245
Independent reflections	6195 (R_{int} = 0.0322)	7789 (R_{int} = 0.0257)	10 855 (R_{int} = 0.0330)
R_1, wR_2 [$I > 2\sigma(I)$]	0.0430, 0.1071	0.0594, 0.1613	0.0337, 0.0883
R_1, wR_2 (all data)	0.0502, 0.1110	0.0759, 0.1698	0.0407, 0.0916
Largest diff. peak and hole (eÅ^{-3})	1.861 and −2.893	2.603 and −2.989	3.670 and −2.723

continuation of the synthesis of new organic–inorganic borotungstate-based hybrids, we continued to explore the assembly of borotungstates in the presence of transition-metal and organic ligands under hydrothermal conditions. Herein, we reported three novel organic–inorganic hybrid borotungstates $\{[Ni(phen)_2(H_2O)]_2H(\alpha\text{-}BW_{12}O_{40})\}\cdot 4H_2O$ (**1**), $[Cu^I(2,2'\text{-bipy})(4,4'\text{-bipy})_{0.5}]_2$ $\{[Cu^I(2,2'\text{-bipy})]_2Cu^I$ $(4,4'\text{-bipy})_2(\alpha\text{-}BW_{12}O_{40})\}$ (**2**) and $\{[Cu^I(4,4'\text{-bipy})]_3H_2(\alpha\text{-}BW_{12}O_{40})\}\cdot 3.5H_2O$ (**3**) (phen = 1,10-phenanthroline, 2,2′-bipy = 2,2′-bipyridine, 4,4′-bipy = 4,4′-bipyridine). Interestingly, the combination of in situ formed borotungstates and transition-metal complexes realize the assembly of 0-D, 1-D to 2-D structures. Moreover, the presence of Ni^{II} and W^{VI} in **1**, Cu^I ions and W^{VI} in **2** and **3** are identified by XPS (X-ray photoelectron spectroscopy) spectra. The photoluminescence of **2** and **3** are also investigated.

2. Experimental

2.1. Materials and methods

All reagents were purchased from commercial sources and used without further purification. IR spectra were recorded on a Nicolet 170 FT-IR spectrometer using KBr pellets in the range of 4000–400 cm^{-1}. UV spectra were obtained on a Unican UV-500 spectrometer (distilled water as solvent) in the range of 400–190 nm. C, H and N elemental analyses were performed on a Perkin-Elmer 2400C elemental analyzer. XPS analyses were performed on an AXIS ULTRA spectrometer with an Al$K\alpha$ achromatic X-ray source. Emission/excitation spectra were recorded on an F-7000 fluorescence spectrophotometer. PXRD (powder X-ray diffraction) were obtained using a Philips X′Pert-MPD diffractometer with Cu$K\alpha$ radiation (λ = 1.54056 Å). TGA (thermogravimetric analysis) curves were recorded with Perkin-Elmer-7 instrument under N_2 atmosphere with a heating rate of 10 °C/min.

2.2. Synthesis

2.2.1. Synthesis of $\{[Ni(phen)_2(H_2O)]_2H(\alpha\text{-}BW_{12}O_{40})\}\cdot 4H_2O$ (**1**)

A mixture of H_3BO_3 (1.5 mmol, 0.093 g), $Na_2WO_4\cdot 2H_2O$ (15 mmol, 4.948 g), phen (1.5 mmol, 0.174 g), $NiSO_4\cdot 6H_2O$ (3.0 mmol, 0.789 g) and distilled water (1 mol, 18 mL) was stirred for 4 h in air, and its pH was adjusted to 2.83 with hydrochloric acid (6 mol L^{-1}). The resulting mixture was sealed in a 40 mL Telfon-lined reactor, heated to 180 °C and kept for 2 days. After cooling to room temperature at 5 °C/h, purple block crystals were collected in 30% yield (based on $NiSO_4\cdot 6H_2O$), by filtration, washed with distilled water, and dried at ambient temperature. Anal. calcd. for **1** (%): C, 14.93; H, 1.32; N, 2.90. Found: C, 14.80; H, 1.24; N, 2.95.

2.2.2. Synthesis of $[Cu^I(2,2'\text{-bipy})(4,4'\text{-bipy})_{0.5}]_2\{[Cu^I(2,2'\text{-bipy})]_2Cu^I(4,4'\text{-bipy})_2(\alpha\text{-}BW_{12}O_{40})\}$ (**2**)

A mixture of H_3BO_3 (1.5 mmol, 0.093 g), $Na_2WO_4\cdot 2H_2O$ (18 mmol, 5.94 g), 2,2′-bipy (0.5 mmol, 0.078 g), 4,4′-bipy (0.67 mmol, 0.129 g), $Cu(CH_3COO)_2\cdot H_2O$ (3 mmol, 0.589 g) and H_2O (1 mol, 18 g) was stirred for 4 h in air. Then the pH was adjusted to 6.40 with acetic acid. The mixture was then transferred to a 40 mL Teflon-lined autoclave and kept at 160 °C for 4 days. After slowly cooling to room temperature at 5 °C/h, orange block crystals of **2** were collected by filtration, washed with distilled water, and dried at ambient temperature (yield: 50% based on $Cu(CH_3COO)_2\cdot H_2O$). Anal. calcd. for **2** (%): C, 19.68; H, 1.31; N, 4.59. Found: C, 19.66; H, 1.43; N: 4.39.

2.2.3. Synthesis of $\{[Cu^I(4,4'\text{-bipy})]_3H_2(\alpha\text{-}BW_{12}O_{40})\}\cdot 3.5H_2O$ (**3**)

Compound **3** was prepared in a manner similar to compound **2** except that pH was adjusted to 4.10 (yield: 40% based on $Cu(CH_3COO)_2\cdot H_2O$). Anal. calcd. for **3** (%): C, 10.05; H, 0.92; N, 2.35. Found: C, 9.92; H, 0.84; N, 2.40.

2.3. X-ray crystallographic analysis

Crystal data for compounds **1**–**3** were collected at 296(2) K on Bruker APEX-II CCD detector with graphite monochromatic Mo$K\alpha$ radiation (λ = 0.71073 Å). Intensity data were corrected for Lorentz and polarization effects. The structures were solved by direct methods and refined by full-matrix least-squares on F^2 using the SHELXTL-97 program [47]. All the non-hydrogen atoms were refined anisotropically. All the hydrogen atoms were placed

in idealized positions and refined with a riding model using default SHELXL parameters. Those hydrogen atoms attached to lattice water molecules were not located. Crystallographic data and structure refinements for **1**–**3** were summarized in Table 1. Selected bond lengths (Å) and angles (°) for **1**–**3** were listed in Table 2.

3. Results and discussion

3.1. Synthesis

During the course of exploring the assembly of borotungstates and transition-metal complexes under hydrothermal conditions, we firstly discovered $[Mn(2,2'\text{-bipy})_3]_{1.5}[BW_{12}O_{40}Mn(2,2'\text{-bipy})_2(H_2O)]\cdot 0.25H_2O$ (**4**), $[Fe(2,2'\text{-bipy})_3]_{1.5}[BW_{12}O_{40}Fe(2,2'\text{-bipy})_2(H_2O)]\cdot 0.5H_2O$ (**5**) and $[Cu_2(phen)_2(OH)_2]_2H[Cu(H_2O)_2\{BW_{12}O_{40}\text{-}Cu_{0.75}(phen)(H_2O)\}_2]\cdot 1.5H_2O$ (**6**) [46]. In order to introduce other transition metals of the first row (e.g. Cr, Co, Ni, Zn, etc.) into this system, many experiments have been done. When $NiSO_4\cdot 6H_2O$ was employed, the 0-D hybrid **1** was obtained. However, those Cr, Co or Zn containing species have not been separated so far. The continuous efforts are in progress. Because the above-mentioned compounds are all isolated structure and each contains one kind of organic ligands, to prepare some novel high-dimensional organic–inorganic hybrid materials with mixed organic ligands based on borotungstates and transition-metal complexes, the copper ions were introduced into this system based on two reason: (a) the copper ions display the evident Jahn–Teller effect in the crystal filed, which can lead to the coordination polyhedral distortion and allow the existence of the longer Cu–O bonds and (b) the copper ions have rich coordination geometries such as two-coordinate linear-type, three-coordinate T-type, four-coordinate tetrehedral geometry, five-coordinate square-pyramid geometry and six-coordination octahedral geometry. When 2,2′-bipy and 4,4′-bipy were simultaneously introduced, the 1-D hybrid **2** was successfully isolated. In the course of investigating the influence of the pH value on the structure of **2**, the 2-D hybrid **3** was unexpectedly obtained. The main difference between **2** and **3** is that (1) **2** is 1-D chain structure whereas **3** is 2-D sheet structure and (2) **2** contains two types of organic ligands while **3** only contains one type of ligand. It should be noted that the organic components not only function as the functional ligands, but also part organic components act as the reduction agent in the formation of **2** and **3**. The comparison of synthetic conditions between **2** and **3** explains that the pH value plays an important role in the formation of **2** and **3**. The comparisons of synthetic conditions of **1**–**6** (Table 3) reveal that the $[\alpha\text{-}BW_{12}O_{40}]^{5-}$ polyoxoanion can exist in the wide pH range.

3.2. Structural description

In order to confirm the purity of **1**–**3**, the powder X-ray diffraction measurements have been performed. The results show that the powder X-ray diffraction patterns of the bulk products of **1**, **2** and **3** are in good agreement with the calculated patterns based on the results from single-crystal X-ray diffraction, which indicate the bulk products for **1**, **2** and **3** are pure (Fig. S1). The differences in intensity may be due to the preferred orientation of the powder samples. Compounds **1**, **2** and **3** crystallize in the triclinic space group *P*-1, although their structures are different. Their common structural features are that they all contain the classic Keggin polyoxoanions $[\alpha\text{-}BW_{12}O_{40}]^{5-}$ as the fundamental building blocks. For **1**–**3**, the W–O bond lengths are 1.672(9)–1.707(8), 1.655(10)–1.7023(148) and 1.700(5)–1.719(6) Å for the terminal oxygen atoms ($W\text{–}O_t$); 1.725(13)–2.133(13), 1.832(14)–1.941(11) and 1.865(5)–1.956(5) Å for the bridging oxygen atoms ($W\text{–}O_{b,c}$); and 2.343(11)–2.502(12), 2.357(16)–2.52(2) and 2.331(5) –2.390(4) Å for the central oxygen atoms ($W\text{–}O_a$), respectively. The B–O distances are in the range of 1.483(11)–1.553(8), 1.470(16)–1.58(2) and 1.518(9)–1.538(8) Å for **1**–**3**, respectively, and the O–B–O angles are in the range of 65.7(6)–114.3(6), 67.4(10)–112.6(10) and 70.1(10)–112.6(10)° for **1**–**3**, respectively. These are good consistent with the previous

Table 2
Selected bond lengths (Å) and angles (°) for **1**–**3**.

1					
B1–O3	1.553(8)	B1–O13	1.483(11)	W1–O4	2.429(12)
W2–O8	1.707(8)	W3–O16	1.691(8)	W4–O17	1.672(9)
W5–O20	1.686(8)	W6–O10	2.382(11)	Ni1–N3	2.051(8)
Ni1–N1	2.071(7)	Ni1–N4	2.063(8)	Ni1–N2	2.087(8)
Ni1–O1	2.090(7)	Ni1–O1W	2.075(7)		
O13#1–B1–O10	65.7(6)	O13–B1–O4#1	109.4(6)	O10–B1–O4#1	113.5(6)
N3–Ni1–N4	80.7(3)	N3–Ni1–N1	93.0(3)	N4–Ni1–N1	94.3(3)
N4–Ni1–O1W	92.7(3)	N1–Ni1–O1W	171.5(3)		
2					
B1–O19	1.470(16)	B1–O20	1.58(2)	W1–O20	2.350(18)
W2–O2	1.655(10)	W3–O3	1.692(11)	W4–O19	2.464(18)
W5–O22	2.389(19)	W6–O20	2.396(19)	Cu1–N1	2.005(12)
Cu1–N2	2.181(13)	Cu1–N3	1.922(11)	Cu2–N4	1.915(13)
Cu2–O1	2.7262(149)	Cu3–N7	1.890(15)	Cu3–N5	1.929(16)
Cu3–N6	2.091(14)	O19–B1–O20	71.0(10)	N1–Cu1–N3	157.5(5)
N1–Cu1–N2	80.5(5)	N4–Cu2–O1	92.601(531)	N7–Cu3–N5	158.1(7)
N5–Cu3–N6	82.7(6)				
3					
B1–O38	1.538(8)	B1–O40	1.518(9)	W1–O1	1.706(6)
W2–O32	1.926(5)	W3–O3	1.722(5)	W4–O38	2.349(4)
W5–O5	1.719(6)	W6–O38	1.719(6)	W7–O39	2.351(5)
W8–O8	1.718(5)	W9–O9	1.708(6)	W10–O10	1.707(5)
W11–O11	1.718(6)	W12–O12	1.710(6)	Cu1–N1	1.909(6)
Cu1–N3	1.911(6)	Cu1–O5	2.336(6)	Cu2–N2	1.909(6)
Cu2–O4#2	2.5923(52)	Cu2–O11#3	2.7614(75)	O37–B1–O38	109.0(5)
O40–B1–O39	109.9(5)	N1–Cu1–N3	167.6(3)	N1–Cu1–O5	99.1(3)

Symmetry codes: #1: $-x$, $-y+1$, $-z+2$; #2: $-x$, $2-y$, $2-z$; #3:$-x$, $1-y$, $2-z$.

Table 3
The comparisons of synthetic conditions of **1–6**.

Reactant and molar ratio	Temperature/°C	pH	Product
$H_3BO_3/Na_2WO_4 \cdot 2H_2O$/phen/$NiSO_4 \cdot 6H_2O/H_2O$ = 1.5/15/1.5/3.0/1000	180	2.83	**1**
$H_3BO_3/Na_2WO_4 \cdot 2H_2O$/2,2′-bipy/4,4′-bipy/$Cu(CH_3COO)_2 \cdot H_2O/H_2O$ = 1.5/18.0/0.5/0.67/3.0/1000	160	6.40	**2**
$H_3BO_3/Na_2WO_4 \cdot 2H_2O$/2,2′-bipy/4,4′-bipy/$Cu(CH_3COO)_2 \cdot H_2O/H_2O$ = 1.5/18/0.5/0.67/3.0/1000	160	4.10	**3**
$H_3BO_3/Na_2WO_4 \cdot 2H_2O$/2,2′-bipy/$MnSO_4 \cdot H_2O/Mn(CH_3COO)_2 \cdot 4H_2O/NaCH_3COO \cdot 3H_2O/H_2O$ = 12.0/2.0/0.3/0.3/0.5/1.0/833	160	4.80	**4**
$H_3BO_3/Na_2WO_4 \cdot 2H_2O$/2,2′-bipy/$FeSO_4 \cdot 7H_2O/NaCH_3COO \cdot 3H_2O/H_2O$ = 12.0/2.0/0.3/1.0/1.0/833	160	4.50	**5**
$H_3BO_3/Na_2WO_4 \cdot 2H_2O$/phen/$CuSO_4 \cdot 5H_2O/Cu(CH_3COO)_2 \cdot H_2O/NaCH_3COO \cdot 3H_2O/H_2O$ = 10.0/1.5/0.4/1.0/1.0/833	180	3.60–4.00	**6**

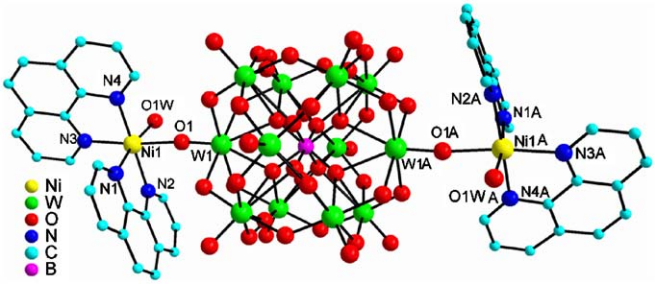

Fig. 1. Ball-and-stick representation of the molecular structure of **1**. The H atoms and lattice water molecules are omitted for clarity. The atoms with the suffix A is generated by the symmetry operation: A: $-x$, $1-y$, $2-z$.

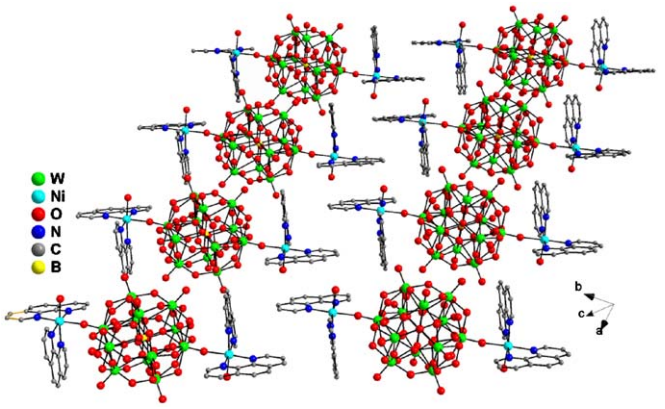

Fig. 2. The supramolecular packing of **1**. The H atoms and the lattice water molecules are omitted for clarity.

results [46]. Notably, different from **3**, in the polyoxoanions $[\alpha\text{-}BW_{12}O_{40}]^{5-}$ of **1** and **2**, the central BO_4 groups are disordered. For the BO_4 group in **1**, four oxygen atoms are all disordered over two positions for each four oxygen atoms while for the BO_4 group in **2**, only two oxygen atoms are disordered over two positions, respectively. Similar disordered phenomena have been reported in the previous studies [48–51].

The molecular structure of **1** are composed of a bisupporting hybrid polyoxoanion $\{[Ni(phen)_2(H_2O)]_2(\alpha\text{-}BW_{12}O_{40})\}^{-}$, one proton and four crystallization water molecules. The molecular structure of **1** is centrosymmetrical, where the boron atom is situated on the inversion center (0, 0.5, 1.0). As shown in Fig. 1, the new $\{[Ni(phen)_2(H_2O)]_2(\alpha\text{-}BW_{12}O_{40})\}^{-}$ hybrid polyoxoanion consists of a Keggin-type polyoxoanion $[\alpha\text{-}BW_{12}O_{40}]^{5-}$ and two supporting $\{Ni(phen)_2(H_2O)\}^{2+}$ coordination cations. The $[\alpha\text{-}BW_{12}O_{40}]^{5-}$ polyoxoanion is covalently bonded to two coordination cations $\{Ni(phen)_2(H_2O)\}^{2+}$ via two terminal oxygen atoms (O1 and O1A). Therefore, the polyoxoanion $[\alpha\text{-}BW_{12}O_{40}]^{5-}$ acts as a special didentate ligand toward two Ni^{2+} ions. The Ni^{2+} ions in the hybrid polyoxoanion $\{[Ni(phen)_2(H_2O)]_2(\alpha\text{-}BW_{12}O_{40})\}^{-}$ exhibits a slightly distorted octahedral geometry, which is defined by four nitrogen atoms from two 1,10-phen ligands with the Ni–N distances of 2.051(8)–2.087(8) Å and the N–Ni–N angles of 80.7(3)–173.4(3)°, one oxygen atom from one terminal (O1) of the $[\alpha\text{-}BW_{12}O_{40}]^{5-}$ polyoxoanion with the Ni–O distance of 2.090(7) Å, and one oxygen atom from the water molecule, with the Ni–O distance of 2.075(7) Å. Adjacent bisupporting hybrid polyoxoanions $\{[Ni(phen)_2(H_2O)]_2(\alpha\text{-}BW_{12}O_{40})\}^{-}$ are stably packed together constructing the extended supramolecular structure via the off-set face-to-face π–π stacking interactions between adjacent phen molecules with a plane-to-plane separation of ca. 3.5 Å (Fig. 2).

As shown in Fig. 3, the molecular structural unit of **2** contains a Keggin-type polyoxoanion $[\alpha\text{-}BW_{12}O_{40}]^{5-}$, a novel tri-$Cu^{I}$ coordination cation $\{[Cu^{I}(2,2'\text{-bipy})]_2Cu^{I}(4,4'\text{-bipy})_2\}^{3+}$ with two mixed ligands and a discrete di-Cu^{I} coordination cation $[Cu_2(2,2'\text{-bipy})_2(4,4'\text{-bipy})]^{2+}$ with two mixed ligands. Three crystallographically independent Cu^{I} ions in the asymmetrical unit of **2** show two kinds of coordination geometries. The Cu1 ion employs

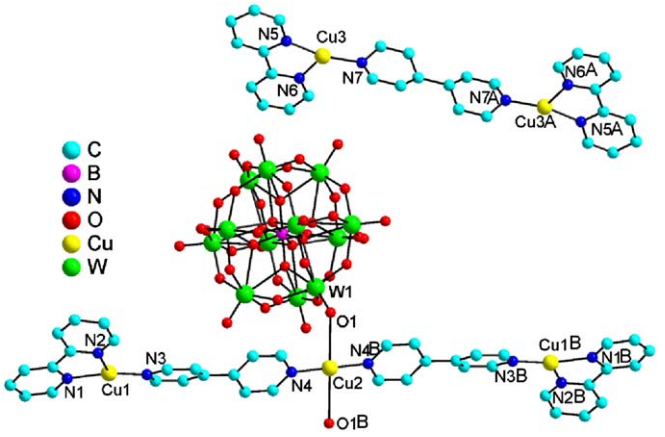

Fig. 3. Ball-and-stick view of the structural unit of **2**. The atoms with the suffix A and B are generated by the symmetry operation: A: $2-x$, $1-y$, $1-z$; B: $-x$, $1-y$, $-z$. All H atoms are omitted for clarity.

the trigonal geometry constituted by three nitrogen (N1, N2 and N3) donors, two of which are from one 2,2′-bipy ligand [Cu–N: 2.005(12)–2.181(13) Å] and one from one 4,4′-bipy ligand [Cu–N: 1.922(11) Å]. The Cu2 ion resides in the square geometry, in which two nitrogen atoms (N4, N4B) from two 4,4′-bipy ligands [Cu–N: 1.915(13) Å], two oxygen atoms (O1, O1B) from two $[\alpha\text{-}BW_{12}O_{40}]^{5-}$ clusters [Cu–O: 2.726(15) Å]. Similar to the Cu1 ion, the Cu3 ion is also the trigonal geometry coordinated by three nitrogen (N5, N6 and N7) donors, two of which are from one 2,2′-bipy ligand [Cu–N: 1.929(16)–2.091(14) Å] and one from one 4,4′-bipy ligand [Cu–N: 1.890(15) Å].

It is interesting that adjacent $[\alpha\text{-}BW_{12}O_{40}]^{5-}$ polyoxoanions are interconnected together through novel trinuclear Cu^{I} coordination cations $\{[Cu^{I}(2,2'\text{-bipy})]_2Cu^{I}(4,4'\text{-bipy})_2\}^{3+}$ constructing a 1-D linear chain architecture (Fig. 4). In this 1-D chain, the $[\alpha\text{-}BW_{12}O_{40}]^{5-}$ polyoxoanion acts as a bidentate inorganic ligand

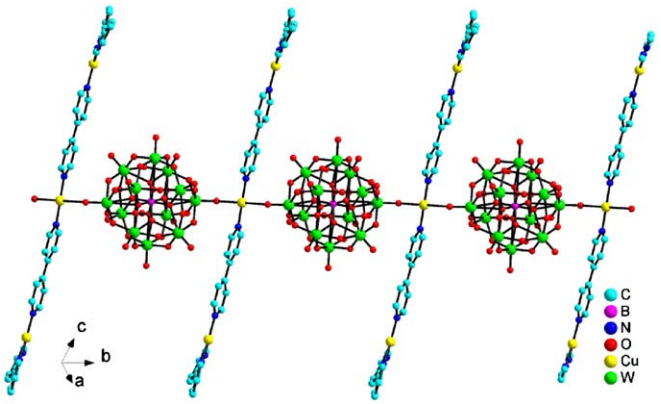

Fig. 4. View of the 1-D chain constructed by alternate $[\alpha\text{-}BW_{12}O_{40}]^{5-}$ clusters and $\{[Cu^{I}(2,2'\text{-bipy})]_2\ Cu^{I}(4,4'\text{-bipy})_2\}^{3+}$ cations in **2**. All H atoms are omitted for clarity.

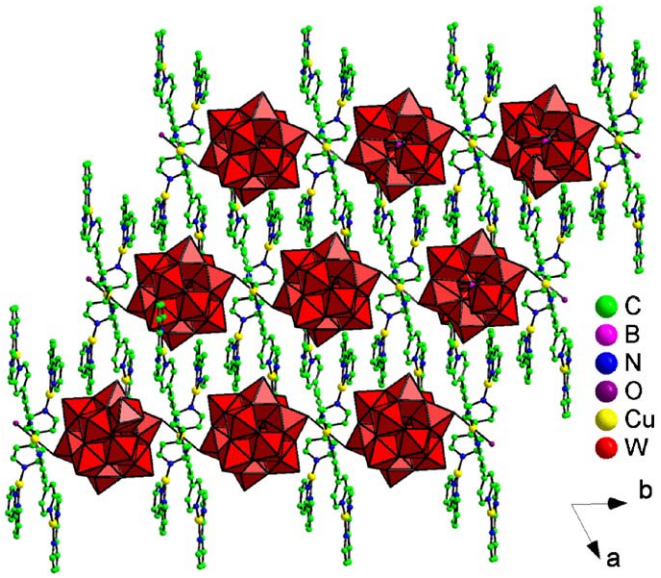

Fig. 5. The 2-D supramolecular arrangement of **2**. The H atoms and the lattice water molecules are omitted for clarity.

providing two terminal oxygen atoms on the opposite site. Through face-to-face π–π interactions between 2,2′-bipy groups [plane-to-plane separation: ca. 3.6 Å] from the supporting $[Cu^{I}(2,2'\text{-bipy})]_2$ $[Cu^{I}(4,4'\text{-bipy})_2]^{3+}$ fragments and the discrete $[Cu_2(2,2'\text{-bipy})_2\ (4,4'\text{-bipy})]^{2+}$ cations, the two-dimensional supramolecular layer can be formed (Fig. 5).

In comparison with **1**, three striking features are observed in **2**: (a) there is a discrete dimeric cation $[Cu_2(2,2'\text{-bipy})_2(4,4'\text{-bipy})]^{2+}$ with two mixed ligands in **2**; (b) the supporting metal coordination complex in **2** is a novel tri-Cu^{I} coordination cation $\{[Cu^{I}(2,2'\text{-bipy})]_2Cu^{I}(4,\ 4'\text{-bipy})_2\}^{3+}$; (c) **2** displays a 1-D linear chain architecture built by alternate $[\alpha\text{-}BW_{12}O_{40}]^{5-}$ polyoxoanions and $\{[Cu^{I}(2,2'\text{-bipy})]_2Cu^{I}(4,4'\text{-bipy})_2\}^{3+}$ coordination cations.

The molecular structural unit of **3** is composed of one Keggin-type $[\alpha\text{-}BW_{12}O_{40}]^{5-}$ polyoxoanion, three crystallographically independent Cu^{I} ions, three 4,4′-bipy ligands, two protons, and three and a half crystallization water molecules (Fig. 6). Three crystallographically independent Cu^{I} ions in the asymmetrical unit of **3** also show two kinds of coordination geometries. The Cu1 atom displays the T-type geometry coordinated by two nitrogen atoms from two 4,4′-bipy ligands [Cu–N: 1.909(6)–1.911(6) Å] and one oxygen atom of the $[\alpha\text{-}BW_{12}O_{40}]^{5-}$ polyoxoanion [Cu–O:

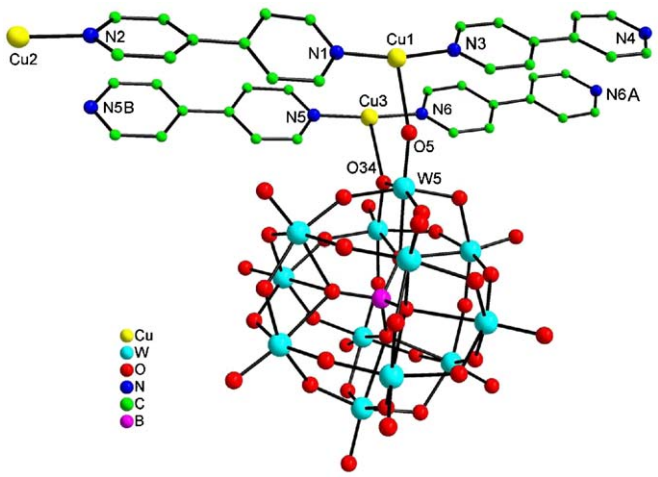

Fig. 6. Ball-and-stick view of the structural unit of **3**. The H atoms are omitted for clarity.

2.336(6) Å]. The Cu2 atom adopts a distorted square coordination geometry established by two nitrogen atoms from two 4,4′-bipy ligands [Cu–N: 1.909(6)–1.914(7) Å] and two oxygen atoms of two different $[\alpha\text{-}BW_{12}O_{40}]^{5-}$ polyoxoanions [Cu–O: 2.592(5)–2.761(7) Å]. Similar to the Cu1 ion, the Cu3 ion also displays a T-type geometry defined by two nitrogen atoms from two 4,4′-bipy ligands [Cu–N: 1.902(6)–1.913(6) Å] and one oxygen atom of the $[\alpha\text{-}BW_{12}O_{40}]^{5-}$ polyoxoanion [Cu–O: 2.580(6) Å].

The most intriguing feature of **3** is the novel 2-D sheet structure (Fig. 7) constructed by $[\alpha\text{-}BW_{12}O_{40}]^{5-}$ polyoxoanions and two types of $-Cu^{I}$–4,4′-bipy– 1-D polymeric chains [namely, $\{-4,4'\text{-bipy}-Cu1-4,4'\text{-bipy}-Cu2-\}_n$ (Fig. S2a) and $\{-4,4'\text{-bipy}-Cu3-4,4'\text{-bipy}-\}_n$ (Fig. S2b)] through the bridging role of the tetradentate $[\alpha\text{-}BW_{12}O_{40}]^{5-}$ polyoxoanions (Fig. S3). In the 2-D structure, each Cu1 ion links one $[\alpha\text{-}BW_{12}O_{40}]^{5-}$ polyoxoanion through a terminal oxygen atom and all the Cu1 ions protrude one side of the $\{-4,4'\text{-bipy}-Cu1-4,4'\text{-bipy}-Cu2-\}_n$ chain (Fig. S2a); each Cu2 ion links two symmetric $[\alpha\text{-}BW_{12}O_{40}]^{5-}$ polyoxoanions projecting toward two sides of the $\{-4,4'\text{-bipy}-Cu1-4,4'\text{-bipy}-Cu2-\}_n$ chain through two terminal oxygen atoms; however, each Cu3 atom links one $[\alpha\text{-}BW_{12}O_{40}]^{5-}$ polyoxoanion through one bridging oxygen atom and neighboring $[\alpha\text{-}BW_{12}O_{40}]^{5-}$ polyoxoanion in the $\{-4,4'\text{-bipy}-Cu3-4,4'\text{-bipy}-\}_n$ chain project toward two sides of the chain (Fig. S2b). Another fascinating structural feature of **3** is that the $[\alpha\text{-}BW_{12}O_{40}]^{5-}$ sphere is modified in an unusually asymmetrical mode as shown in Fig. 7. Each $[\alpha\text{-}BW_{12}O_{40}]^{5-}$ sphere acts as a tetradentate inorganic ligand (Fig. S3) providing four O atoms, three of which are the terminal O atoms (O4, O5 and O11) and one is the bridging O atom (O34). In this mode, each $[\alpha\text{-}BW_{12}O_{40}]^{5-}$ sphere is combined with four $-Cu^{I}$–4,4′-bipy– polymeric chains, three of which are the $\{-4,4'\text{-bipy}-Cu1-4,4'\text{-bipy}-Cu2-\}_n$ chains, and one is the $\{-4,4'\text{-bipy}-Cu3-4,4'\text{-bipy}-\}_n$ chain. Therefore, four $-Cu^{I}$–4,4′-bipy– chains are joined together by $[\alpha\text{-}BW_{12}O_{40}]^{5-}$ spheres to build up a rail-like chain, in which the $[\alpha\text{-}BW_{12}O_{40}]^{5-}$ spheres looks like the middle rail. The adjacent "rails" are linked via sharing three $-Cu^{I}$–4,4′-bipy– chains to form the sheet 2-D structure. Although the connecting fashion between $[\alpha\text{-}BW_{12}O_{40}]^{5-}$ spheres and $-Cu^{I}$–4,4′-bipy– chains is very similar with that between $[GeMo_{12}O_{40}]^{4-}$ spheres and $-Cu^{I}$–4,4′-bipy– chains in $\{[Cu(4,4'\text{-bipy})]_3[HGe\ Mo_{12}O_{40}]\}\cdot 0.5H_2O$ reported by Peng et al. [25], two obvious differences exist between them: (a) the $[\alpha\text{-}BW_{12}O_{40}]^{5-}$ sphere is a tetradentate ligand bonding to four $-Cu^{I}$–4,4′-bipy– chains in the former, while the $[GeMo_{12}O_{40}]^{4-}$

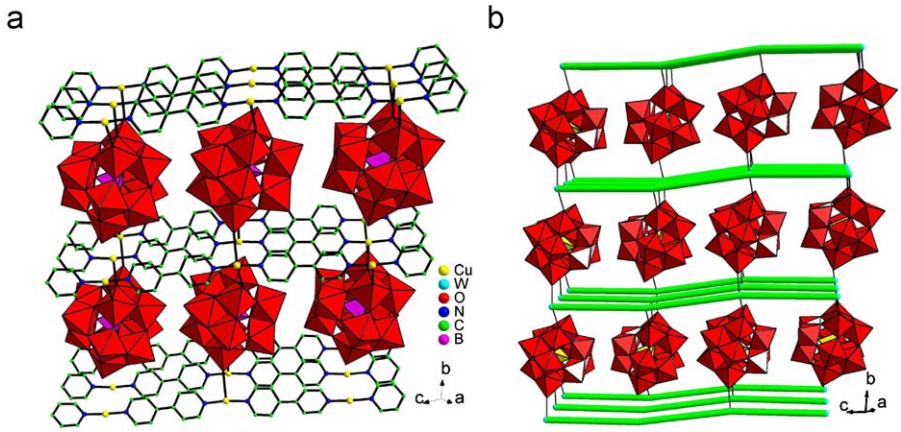

Fig. 7. (a) The polyhedral/ball-and-stick view of the 2-D sheet structure of **3** constructed by $[\alpha\text{-}BW_{12}O_{40}]^{5-}$ polyoxoanions and two types of 1-D –Cu^{I}–4,4′-bipy– polymeric chains through the bridging role of the tetradentate $[\alpha\text{-}BW_{12}O_{40}]^{5-}$ polyoxoanions. (b) The polyhedral/wire view of the 2-D structure of **3**. The –Cu^{I}–4,4′-bipy– polymeric chains are shown in green bars. Color code: WO_6 octahedra, red; BO_4 tetrahedra, purple; Cu atoms, yellow; N atoms, blue; C atoms, green. (For interpretation of the references to colour in this figure legend, the reader is referred to the web version of this article.)

sphere is a tridentate ligand bonding to three –Cu^{I}–4,4′-bipy– chains in the latter; (b) the former displays a 2-D sheet structure whereas the latter utilizes a 1-D chain structure. From the viewpoint of topology, the 2-D sheet structure can be viewed as (3,4)-connected topological net, in which the $[\alpha\text{-}BW_{12}O_{40}]^{5-}$ sphere acts as 4-connected node, the Cu1 and Cu3 ions work as 3-connected nodes and the Cu2 ion functions as 4-connected node (Fig. S4). The long topological (O′Keeffe) vertex symbol is $6_2\cdot8_2\cdot8_2\cdot6_2\cdot6_2\cdot6_2$ for the $[\alpha\text{-}BW_{12}O_{40}]^{5-}$ node, $6\cdot6\cdot6_2$ for Cu1 node, $6\cdot8\cdot6_2\cdot6\cdot8_2\cdot6_2$ for the Cu2 node and $6_2\cdot8_2\cdot6_2$ for the Cu3 node, which gives the short vertex (Schäfli) symbol $(6^4\cdot8^2)(6^3)(6^4\cdot8^2)(6^2\cdot8)$.

The BVS values [52–53] of Ni1 ions in **1** are 1.90, Cu1, Cu2, Cu3 in **2** and **3** ions are 0.99, 1.16, 0.97 and 1.02, 1.00, 0.96, respectively, indicating that the oxidation states of Ni1 ions in **1** are +2, the oxidation states of Cu1, Cu2, Cu3 in **2** and **3** are +1, being in good consistence with three-coordinate or four-coordinate coordination geometries and the results of the XPS spectra (Fig. S5). Moreover, the fact that the oxidation states of W atoms in **1**–**3** are +6 are also further identified by XPS spectra (Fig. S5). Since no Cu^{I} ions were used in the starting materials, the Cu^{I} ions in **2** and **3** must be derived from the reduction of Cu^{II} ions in the presence of 2,2′-bpy or 4,4′-bpy as a reductive agent. It is a common phenomenon that the high oxidation state metals are reduced by bipyridine under hydrothermal conditions [54–56].

3.3. IR spectra

The IR spectra of **1**–**3** have been recorded between 4000 and 400 cm^{-1}, which is very useful for identification of the characteristic vibration bands of Keggin polyoxoanions and organic components in products. In the IR spectra of **1**–**3**, four characteristic vibration patterns derived from Keggin-type polyoxoanions are observed in 700–1000 cm^{-1}. Four characteristic peaks at 957, 899, 823 and 724 cm^{-1}; 948, 905, 825 and 764 cm^{-1}; 950, 891, 808 and 720 cm^{-1} are attributed to the $\nu(W\text{–}O_d)$, $\nu(W\text{–}O_a)$, $\nu(W\text{–}O_b)$ and $\nu(W\text{–}O_c)$ stretching vibration, respectively. In comparison with the IR spectra of the parent $\alpha\text{-}H_5BW_{12}O_{40}\cdot30H_2O$ [42], the characteristic $\nu(W\text{–}O_d)$ and $\nu(W\text{–}O_a)$ vibration frequencies in **1**–**3** have red-shifted, the reason of which may be that the metal coordination cations covalently coordinate to the surface of Keggin-type polyoxoanions. However, the vibration frequencies of $\nu(W\text{–}O_b)$ and $\nu(W\text{–}O_c)$ in **1**–**3** have blue-shifted, the reason of which may be the decrease of the symmetry of Keggin-type polyoxoanions in comparison with that in $\alpha\text{-}H_5BW_{12}O_{40}\cdot30H_2O$. In addition, vibration bands in the 1626–1000 cm^{-1} region in **1** are attributed to the phen groups. Vibration bands in the 1600–1060 cm^{-1} region in **2** are assigned to the 2,2′-bipy and 4,4′-bipy groups. Vibration bands in the 1610–1074 cm^{-1} region in **3** are attributed to the 4,4′-bipy groups.

3.4. UV spectra

In order to study the solution optical property of **1**–**3**, their UV spectra are performed in the aqueous solution (Fig. S6). The UV spectra display one strong absorption band and one wide shoulder absorption band in the region of 400–190 nm, appearing at 195 and 280 nm for **1** and 194 and 237 nm for **2**. Their higher energy band can be assigned to $O_d\rightarrow W$ charge transfer absorption band, whereas the lower energy band is attributed to $O_{b(c)}\rightarrow W$ charge transfer transitions, which is characteristic of Keggin-type polyoxoanion [57]. For **3**, only one wide shoulder absorption band attributed to $O_{b(c)}\rightarrow W$ charge transitions is observed at 258 nm in the UV spectrum; however, the strong absorption is blue-shifted to the near-UV region. From the viewpoint of structural chemistry, the red-shift or blue-shift phenomena of the $O_d\rightarrow W$ or $O_{b(c)}\rightarrow W$ charge transfer absorption bands may be related to the interactions between the polyoxoanions and metal-organic cations (mainly including static electronic interaction, covalent bonding interaction and π–π stacking interactions).

3.5. X-ray photoelectron spectroscopy (XPS)

Although the oxidation states of Ni, Cu and W atoms in **1**, **2** and **3** have been determined as +2, +1 and +6, respectively, by means of theoretical BVS calculations, in order to further confirm their oxidation states by means of experimental technique, the XPS measurements of **1**, **2** and **3** are performed (Fig. S5). In **1**, the $Ni2p_{1/2}$ and $Ni2p_{3/2}$ binding energy values of 871.0 and 854.1 eV indicate the presence of the Ni^{II} centers. These values are in good agreement with the values collected in the literatures [58–59]. The spin–orbit components ($2p_{3/2}$ and $2p_{1/2}$) of the Cu2p peak were well deconvoluted by two curves at 932.25 and 952.36 eV with a spin–orbit separation of 20.11 eV for **2**, and 931.38 and 951.55 eV with a spin–orbit separation of 20.17 eV for **3**. The above results confirm the presence of Cu^{I} in **2** and **3**. These values are in

good agreement with the values collected in the literature [60–61]. Furthermore, the typical shake-up lines of Cu^{II} were not observed, indicating that the chemical state of Cu in **2** and **3** is not a bivalent oxidation state. Additionally, the $W4f_{5/2}$ and $W4f_{7/2}$ binding energy values of 34.6 and 36.7 eV for **1**, 34.7 and 36.9 eV for **2**, and 34.5 and 36.6 eV for **3** indicate that all the W^{VI} centers in **1**, **2** and **3** are +6 [62] (Fig. S5). These observations are in good agreement with the results of the single-crystal X-ray analysis and BVS calculations.

3.6. Photoluminescence

The emission and excitation spectra of **2** and **3** in solid state at room temperature are depicted in Fig. 8. Compounds **2** and **3** exhibits obvious photoluminescence in the solid state with a broad emission band at 600 nm upon excitation at about 400 nm for **2** and 610 nm upon excitation at about 405 nm for **3**, respectively. From theoretical considerations, and by comparison with other luminescent Cu^{I} compounds containing amine ligands, the emission is often thought to be related to a mixed excited state of the Cu^{I} ion and ligand-to-metal charge-transfer (MLCT) transitions [61]. The above analysis shows the compound is probably a potential photoactive material.

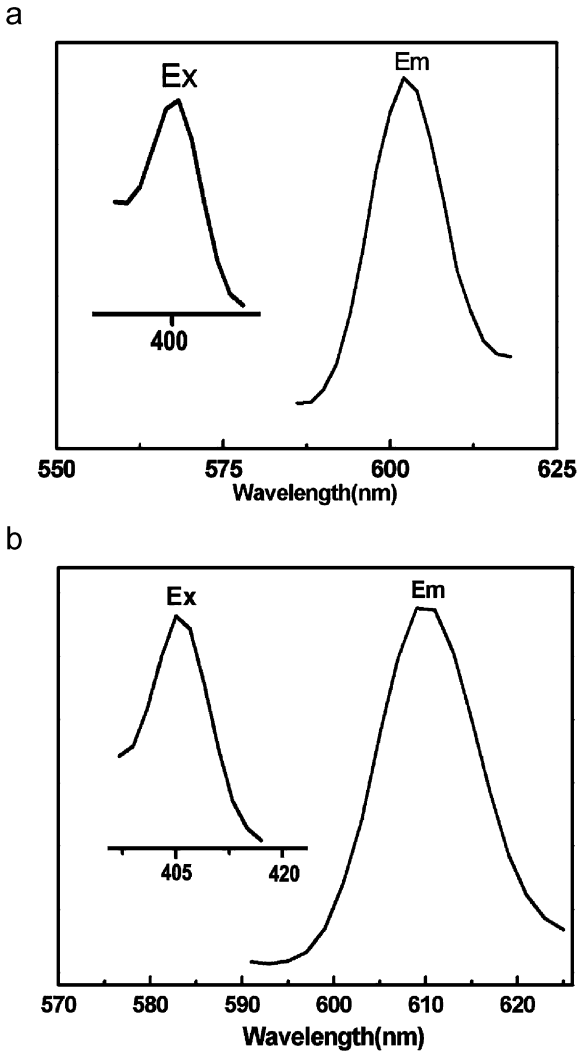

Fig. 8. (a) Emission spectrum (maximum 600 nm) and excitation spectrum (inset, maximum 400 nm) for **2** in the solid state at room temperature. (b) Emission spectrum (maximum 610 nm) and excitation spectrum (inset, maximum 405 nm) for **3** in the solid state at room temperature.

3.7. Thermogravimetric analyses (TGA)

To investigate the thermal stabilities for **1**, **2** and **3**, TGA measurements were performed. **1** shows one slow weight loss step. The weight loss of 23.51% from 30 to 578 °C is attributed to the loss of four crystal water molecules, two coordinate water molecules and four phen molecules and the dehydration of one proton (calcd. 22.02%). For **2**, it exhibits two weight loss steps in the range of 30–549 °C. The weight loss of 14.84% between 30 and 253 °C corresponds to the loss of four organic molecules (calcd. 14.63%). The weight loss of 11.42% between 253 and 549 °C is assigned to the loss of other three organic molecules (calcd. 10.98%). The whole weight loss 26.26% is in good agreement with the calculated value (25.62%). For **3**, it exhibits two continuous slow weight loss steps. The total weight loss of 16.13% in the range of 30–543 °C corresponds to the loss of 3.5 crystal water molecules and three 4,4′-bipy molecules and the dehydration of two protons (calcd. 15.35%) (Fig. S7).

4. Conclusions

Three novel organic–inorganic hybrid borotungstates $\{[Ni(phen)_2(H_2O)]_2H(\alpha\text{-}BW_{12}O_{40})\}\cdot 4H_2O$ (**1**), $[Cu^{I}(2,2'\text{-bipy})(4,4'\text{-bipy})_{0.5}]_2\{[Cu^{I}(2,2'\text{-bipy})]_2Cu^{I}(4,4'\text{-bipy})_2(\alpha\text{-}BW_{12}O_{40})\}$ (**2**) and $\{[Cu^{I}(4,4'\text{-bipy})]_3H_2(\alpha\text{-}BW_{12}O_{40})\}\cdot 3.5H_2O$ (**3**) have been hydrothermally synthesized and structurally characterized. **1** consists of a 0-D bisupporting polyoxometalate cluster where two $[Ni(phen)_2(H_2O)]^{2+}$ cations are grafted on the polyoxoanion $[\alpha\text{-}BW_{12}O_{40}]^{5-}$ through two terminal oxygen atoms. **2** shows a 1-D infinite chain constructed from $[\alpha\text{-}BW_{12}O_{40}]^{5-}$ polyoxoanions and $\{[Cu^{I}(2,2'\text{-bipy})]_2Cu^{I}(4,4'\text{-bipy})_2\}^{3+}$ cations by means of alternating fashion. **3** displays an unprecedented 2-D extended structure built by $[\alpha\text{-}BW_{12}O_{40}]^{5-}$ polyoxoanions and $-Cu^{I}$–4,4′-bipy– linear chains. The combination of in situ formed borotungstates and transition-metal complexes realize the assembly of 0-D, 1-D to 2-D structures. The presence of Ni^{II} and W^{VI} in **1**, Cu^{I} ions and W^{VI} in **2** and **3** are identified by XPS spectra. The photoluminescence of **2** and **3** are also investigated.

Supplementary data

Crystallographic data for the structural analyses reported in this paper has been deposited with the Cambridge Crystallographic Data Centre with the deposited CCDC numbers 706384, 706382 and 706383 for **1**, **2** and **3**. Copies of this information may be obtained free of charge from The Director, CCDC, 12 Union Road, Cambridge CB2 1EZ, UK (fax: +44 1223 336033; e-mail: deposit@ccdc.cam.ac.uk).

Acknowledgments

This work was supported by the National Natural Science Foundation of China, the Program for New Century Excellent Talent in University of Henan Province, the Foundation of Educational Department of Henan Province, and the Natural Science Foundation of Henan Province.

Appendix A. Supplementary material

Supplementary data associated with this article can be found in the online version at 10.1016/j.jssc.2009.04.028.

References

[1] M.T. Pope, Heteropoly and Isopoly Oxometalates, Springer, Berlin, 1983.
[2] V. Soghomonian, Q. Chen, R.C. Haushalter, J. Zubieta, C.J. O'Connor, Science 259 (1993) 1596.
[3] A. Müller, S.Q.N. Shah, H. Bögge, M. Schmidtmann, Nature 397 (1999) 48.
[4] K. Fukaya, T. Yamase, Angew. Chem. Int. Ed. 42 (2003) 654.
[5] X.K. Fang, T.M. Anderson, C.L. Hill, Angew. Chem. Int. Ed. 44 (2005) 3540.
[6] C.D. Wu, C.Z. Lu, H.H. Zhuang, J.S. Huang, J. Am. Chem. Soc. 124 (2002) 3836.
[7] J.R. Galán-Mascarós, C. Giménez-Saiz, S. Triki, C.J. Gómez-García, E. Coronado, L. Ouahab, Angew. Chem. Int. Ed. 34 (1995) 1460.
[8] H.Y. An, Y. Lan, Y.G. Li, E.B. Wang, N. Hao, D.R. Xiao, L.Y. Duan, L. Xu, Inorg. Chem. Commun. 7 (2004) 356.
[9] L.C. Li, D.Z. Liao, Z.H. Jiang, S.P. Yan, Inorg. Chem. 41 (2002) 1019.
[10] B.B. Xu, Z.H. Peng, Y.G. Wei, D.R. Powell, Chem. Commun. (2003) 2562.
[11] M.I. Khan, E. Yohannes, D. Powell, Chem. Commun. (1999) 23.
[12] H.Y. An, Y.G. Li, E.B. Wang, D.R. Xiao, C.Y. Sun, L. Xu, Inorg. Chem. 44 (2005) 6062.
[13] F. Bonhomme, J.P. Larentzos, T.M. Alam, E.J. Maginn, M. Nyman, Inorg. Chem. 44 (2005) 1774.
[14] H.Y. An, D.R. Xiao, E.B. Wang, Y.G. Li, L. Xu, New J. Chem. 29 (2005) 667.
[15] H.Y. An, E.B. Wang, D.R. Xiao, Y.G. Li, L. Xu, Inorg. Chem. Commun. 8 (2005) 267.
[16] S. Bareyt, S. Piligkos, B. Hasenknopf, P. Gouzerh, E. Lacôte, S. Thorimbert, M.J. Malacria, J. Am. Chem. Soc. 127 (2005) 6788.
[17] H.Y. An, Y.Q. Guo, Y.G. Li, E.B. Wang, J. Lü, L. Xu, C.W. Hu, Inorg. Chem. Commun. 7 (2004) 521.
[18] J. Tao, Y. Zhang, M.L. Tong, X.M. Chen, T. Yuen, C.L. Lin, X.Y. Huang, J. Li, Chem. Commun. (2002) 1342.
[19] B.Z. Lin, S.X. Liu, Chem. Commun. (2002) 2126.
[20] C.L. Hill, Chem. Rev. 98 (1998) 1.
[21] X.H. Bu, W. Chen, M. Du, K. Biradha, W.Z. Wang, R.H. Zhang, Inorg. Chem. 41 (2002) 437.
[22] P.J. Hagrman, C. Bridges, J.E. Greedan, J. Zubieta, J. Chem. Soc. Dalton Trans. 17 (1999) 2901.
[23] J. Lü, E.H. Shen, M. Yuan, Y.G. Li, E.B. Wang, C.W. Hu, L. Xu, J. Peng, Inorg. Chem. 42 (2003) 6956.
[24] Y. Lu, E.B. Wang, M. Yuan, G.Y. Luan, Y.G. Li, H. Zhang, C.W. Hu, Y.G. Yao, Y.Y. Qin, Y.B. Chen, J. Chem. Soc. Dalton Trans. (2002) 3029.
[25] J. Sha, J. Peng, A. Tian, H. Liu, J. Chen, P. Zhang, Z. Su, Cryst. Growth Des. 7 (2007) 2535.
[26] J.P. Wang, Z.L. Wang, J.Y. Niu, Polyhedron 23 (2004) 773.
[27] J.Y. Niu, M.L. Wei, J.P. Wang, J. Mol. Struct. 689 (2004) 147.
[28] J.P. Wang, X.Y. Duan, J.Y. Niu, J. Mol. Struct. 692 (2004) 17.
[29] J.Y. Niu, Q.X. Han, J.P. Wang, J. Coord. Chem 56 (2003) 523.
[30] J.P. Wang, M.L. Wei, J.Y. Niu, Inorg. Chem. Commun. 6 (2003) 1272.
[31] J.P. Wang, Q. Wu, J.Y. Niu, Chinese Chem. Lett. 13 (2002) 915.
[32] Y. Xu, J.Q. Xu, K.L. Zhang, X.Z. You, Chem. Commun. (2000) 153.
[33] Y.M. Xie, Q.S. Zhang, Z.G. Zhao, X.Y. Wu, S.C. Chen, C.Z. Lu, Inorg. Chem. 47 (2008) 8086.
[34] E. Coronado, C. Giménez-Saiz, C.J. Gómez-García, S.C. Capelli, Angew. Chem. Int. Ed. 43 (2004) 3021.
[35] Y. Ishii, Y. Takenaka, K. Konishi, Angew. Chem. Int. Ed. 43 (2004) 2702.
[36] M. Nyman, F. Bonhomme, T.M. Alam, M.A. Rodriguez, B.R. Cherry, J.L. Krumhansl, T.M. Nenoff, A.M. Sattler, Science 297 (2002) 996.
[37] A. Dolbecq, P. Mialane, L. Lisnard, J. Marrot, F. Sécheresse, Chem. Eur. J. 9 (2003) 2914.
[38] P.Q. Zheng, Y.P. Ren, L.S. Long, R.B. Huang, L.S. Zheng, Inorg. Chem. 44 (2005) 1190.
[39] F. Ortéga, M.T. Pope, Inorg. Chem. 23 (1984) 3292.
[40] N. Haraguch, Y. Okaue, T. Isobe, Y. Matsuda, Inorg. Chem. 33 (1994) 1015.
[41] N. Leclerc-Laronze, J. Marrot, R. Thouvenot, G. Hervé, E. Cadot, Chem. Eur. J. 13 (2007) 7234.
[42] J.Y. Niu, J.W. Zhao, J.P. Wang, P.T. Ma, J. Mol. Struct. 699 (2004) 85.
[43] J.P. Wang, J. Li, J.Y. Niu, Sci. China Ser. B Chem. 36 (2006) 1.
[44] H.Y. An, E.B. Wang, D.R. Xiao, Y.G. Li, Z.M. Su, L. Xu, Angew. Chem. Int. Ed. 45 (2006) 904.
[45] H.Y. An, E.B. Wang, Y.G. Li, Z.M. Zhang, L. Xu, Inorg. Chem. Commun. 10 (2007) 299.
[46] J.P. Wang, G.L. Guo, J.Y. Niu, J. Mol. Struct. 885 (2008) 161.
[47] G.M. Sheldrick, SHEXTL-97, Programs for Crystal Structure Refinements, University of Göttingen, Germany, 1997.
[48] L.-Y. Dai, Y.-K. Shan, M.-Y. He, J. Mol. Struct. 644 (2003) 165.
[49] Y. Lu, E. Wang, Y. Guo, X. Xu, L. Xu, J. Mol. Struct. 737 (2005) 183.
[50] N. Hao, C. Qin, Y. Xu, E. Wang, Y. Li, E. Shen, L. Xu, Inorg. Chem. Commun. 8 (2005) 592.
[51] Y. Xu, L. Nie, G. Zhang, Q. Chen, X. Zheng, Inorg. Chem. Commun. 9 (2006) 329.
[52] N.E. Brese, M. O'Keeffe, Acta Crystallogr. B 47 (1991) 192.
[53] I.D. Brown, D. Altermatt, Acta Crystallogr. B 41 (1985) 244.
[54] H. Jin, Y.F. Qi, E.B. Wang, Y.G. Li, C. Qin, X.L. Wang, S. Chang, Eur. J. Inorg. Chem. (2006) 4541.
[55] W. Yang, C. Lu, H. Zhuang, J. Chem. Soc. Dalton Trans. (2002) 2879.
[56] K.T. Potts, C.P. Horwitz, A. Fessak, M. Keshavarz-K, K.E. Nash, P.J. Toscano, J. Am. Chem. Soc. 115 (1993) 10444.
[57] E.B. Wang, G.P. Wang, R.D. Huang, Sci. Bull. 37 (1992) 1195.
[58] D. Xiao, Y. Li, E. Wang, S. Wang, Y. Hou, G. De, C. Hu, Inorg. Chem. 42 (2003) 7652.
[59] G.-G. Gao, L. Xu, W.-J. Wang, X.-S. Qu, H. Liu, Y.-Y. Yang, Inorg. Chem. 47 (2008) 2325.
[60] J.-K. Cheng, Y.-B. Chen, L. Wu, J. Zhang, Y.-H. Wen, Z.-J. Li, Y.-G. Yao, Inorg. Chem. 44 (2005) 3386.
[61] M. Brust, P.M. Blass, A.J. Bard, Langmuir 13 (1997) 5602.
[62] I.M. Szilágyi, F. Hange, J. Madarász, G. Pokol, Eur. J. Inorg. Chem. (2006) 3413.